

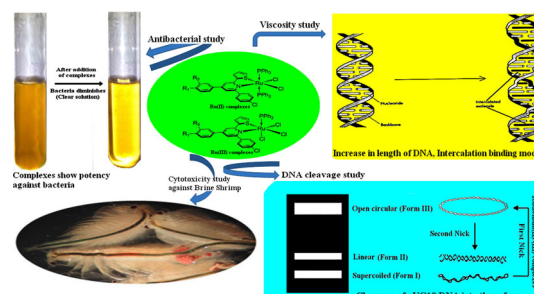
Monitoring the DNA by ruthenium complexes of heterocyclic N,S-donor ligands and evaluation of biological activities

Parag S. Karia¹ · Pankajkumar A. Vekariya¹ · Anshul P. Patidar¹ · Ravi R. Patel² · Mohan N. Patel¹

Received: 28 February 2015 / Accepted: 15 February 2016
© Springer-Verlag Wien 2016

Abstract Neutral N,S-donor bidentate ligands have been synthesized and characterized by NMR and IR spectroscopic techniques. The ligands have been used to synthesize ruthenium(II) complexes ($[\text{Ru}(\text{L}^1\text{-L}^6)\text{PPh}_3)_2\text{Cl}_2]$) and ruthenium(III) complexes ($[\text{Ru}(\text{L}^1\text{-L}^6)\text{PPh}_3)\text{Cl}_3]$). Synthesized complexes have been characterized using elemental analysis, UV–Vis spectroscopy, magnetic measurements, LC–MS, and IR spectroscopy. Broth dilution technique was used to investigate antibacterial activity against two Gram-positive and three Gram-negative microorganisms and results show that all complexes are more potent than the respective ligands. UV–Vis absorption titration and viscosity measurements have been carried out to investigate the binding mode and binding strength of complexes with herring sperm DNA. The quantitative binding strength (K_b) of the complexes was found in the range of 0.521×10^5 – $2.94 \times 10^5 \text{ M}^{-1}$ and indicate intercalative mode of binding. Gel electrophoresis study was carried out to study the cleavage of pUC19 supercoiled DNA. DNA nuclease activity data for the complexes are found higher than respective ligands and metal salt. Brine shrimp bioassay was carried out to perform cytotoxicity study. IC_{50} values of the complexes were found in the range of 5.69 ± 1.06 – $14.62 \pm 0.87 \mu\text{g cm}^{-3}$.

Graphical abstract



Keywords N,S-donor ligands · Ru(II)/Ru(III) complexes · Nucleic acid interaction · Cytotoxicity

Introduction

Current progress in the field of molecular biology has recognized various bioactive compounds that may be logically targeted via inorganic compounds as medication. Metal complexes have come upon as feasible alternatives to organic compounds as scaffolds for the design of molecularly targeted agents due to number of significant advantages [1, 2]. Among these metal compounds, transition metal complexes interacting to DNA have been centre of bioinorganic investigations for at least three decades due to their noteworthy applications in DNA structural probes and molecular switches, disease resistance, development in drug effectiveness, and new drug design and screening [3–6]. Primary importance of using transition metals is owing to variable oxidation states and geometries due to which the coordination sphere of ligands can be rationally

Electronic supplementary material The online version of this article (doi:10.1007/s00706-016-1708-8) contains supplementary material, which is available to authorized users.

✉ Mohan N. Patel
jeenen@gmail.com

¹ Department of Chemistry, Sardar Patel University, Vallabh Vidyanagar 388 120, Gujarat, India

² Department of Bioscience, Sardar Patel University, Vallabh Vidyanagar 388 120, Gujarat, India

planned. This aspect can be exploited to prepare novel structural geometries (e.g. octahedral or square-planar motifs) that are not usually accessible to organic molecules. Second point of selecting transition metal complexes is that the thermodynamic and kinetic properties of these metal complexes are sensitive toward the nature of ligands attached and hence, metal-based therapeutics can be easily optimized to achieve the desired biological applications through alteration of the supporting ligands. In transition metal compounds, platinum based drugs have drawn much attention after the clinical success of cisplatin. However, such metal based drugs are hindered by several problems such as serious toxicity, side effects and major problem with resistance [7]. These unsolved problems in platinum-based anticancer therapy have inspired increased research efforts in the search for new non-platinum-based metal species as cytotoxic agents [8], and currently, there is much interest in the design of ruthenium complexes as anticancer agents [9]. Many Ru(II) and Ru(III) complexes have been reported to exhibit potentially useful cytotoxicity recently, including mer-[Ru(III)(terpy)Cl₃] [10], a-[Ru(II)(azpy)₂Cl₂] [11], and Ru(II) organometallic complexes of the type [(*g*-6-arene)Ru(II)(en)Cl][PF₆] [12]. Most extraordinarily, two other Ru(III) complexes, namely NAMI-A ([ImH][trans-RuCl₄(DMSO)(Im)]) and KP1019 ([IndH][trans-RuCl₄(Ind)₂]) have already entered clinical trials. NAMI-A is nontoxic in vitro while shows very good antimetastatic activity [13]. KP1019 has been introduced into phase I clinical trials against colon carcinomas and their metastases in 2003 [14].

In continuation of our earlier work [15], to understand the role of chelating effect of ligands with ruthenium(II)/(III) in biological application, reaction of N,S-donor ligands derived from pyridinium salt of 2-acetylthiophene and substituted enones, with ruthenium precursor [RuCl₃.PPh₃] has been carried out. Biological activity of the complexes was carried out performing antibacterial, DNA binding, DNA cleavage, and cytotoxicity study.

Results and discussion

Magnetism and electronic spectra

Room temperature magnetic susceptibility of the synthesized complexes has been measured by Gouy's magnetic balance using mercury tetrathiocyanatocobaltate(II) as a calibrant. No change in the weight is observed in the Gouy's balance when the complexes **1–6** were kept in the external magnetic field, indicating the absence of unpaired electron. This also confirms ruthenium in the complexes is in +2 oxidation state. The magnetic moment of complexes **7–12** are found in the range 1.79–1.92 BM. The obtained

values are close to the 1.73 BM indicating that the complexes contain one unpaired electron, with ruthenium ion in its +3 oxidation state.

DMSO was used as a medium to obtain the electronic spectra of the synthesized complexes. In case of ruthenium(II) complexes **1–6**, three distinct bands are observed in the range of 240–800 nm. The band in the range of 262–273 nm is corresponding to intra ligand charge transfer band. The band around 420–440 nm is attributed to metal to ligand charge transfer band. The peak around 550–568 nm is due to *d–d* transition. While in case of ruthenium(III) complexes **7–12**, in the electronic spectra, a band obtained around 270 nm corresponds to intraligand charge transfer band. The band around 350 nm is due to metal-to-ligand charge transfer band. The peak around 540 nm is assigned due to *d–d* transition.

IR spectra

Vibrations modes of the ligands are affected by coordination to ruthenium ion, corresponding to shifting in energy for bands in the IR spectra. These bands are also sensitive to the substituent in the complexes. The IR spectral data obtained due to the chelation of ligands to the ruthenium metal ion are represented in the Supplementary Material. The $\nu(\text{C}=\text{N})$ band of ligands (1390–1397 cm⁻¹) are shifted to higher frequency in complexes (1506–1522 cm⁻¹) suggesting the coordination of ligand through nitrogen atom of pyridine ring [20]. The $\nu(\text{C}=\text{S})$ stretching bands of ligands (1162–1179 cm⁻¹) are shifted to higher frequency (1234–1260 cm⁻¹), which is attributed to the chelation of ruthenium ion to sulfur atom of thiophene ring. Bands observed in the of range 1548–1578 cm⁻¹ assigned as $\nu(\text{C}=\text{C})_{\text{ar}}$ stretching. The $\nu(\text{C}-\text{H})_{\text{ar}}$ stretching bands are observed in the range of 3034–3067 cm⁻¹. Bands observed in the range of 545–572 and 454–475 cm⁻¹ are assigned due to $\nu(\text{Ru}-\text{N})$ and $\nu(\text{Ru}-\text{S})$ stretching vibration, respectively.

Thermal analysis

The TG analyses for complex **1** and complex **7** carried out at a heating rate of 10 °C per minute from ambient temperature to 900 °C under N₂ atmosphere. Thermogram of the complex **1** and complex **7** are represented in the Supplementary Material. In case of complex **1**, no loss in weight is observed up to 170 °C indicating the absence of water molecules. The first loss observed in the temperature range of 180–450 °C is due to the loss of chlorine atoms and triphenylphosphine moiety. The second mass loss occurring in the temperature range of 530–780 °C is attributed to loss of ligand moiety and leaving behind the residue of metal oxide. While in the TG curve of complex

7, no loss in weight is observed up to 160 °C indicating the absence of water molecules. The first mass loss occurs in the temperature range of 170–250 °C, which is attributed to loss of three chlorine atoms, second mass loss occurring in the temperature range of 350–490 °C corresponding to removal of triphenylphosphine moiety and the third mass loss around 580–800 °C is due to decomposition of neutral bidentate ligand, and leaving behind metal oxide as residue.

Mass spectra

Mass spectrum of complex **1** and complex **7** are represented in the Supplementary Material. In the mass spectrum of complex **1**, the peaks at $m/z = 1063.09$, 1065.09 , 1067.01 , and 1069.06 are assigned as molecular ion peak (M^+), ($M + 2$), ($M + 4$), ($M + 6$), respectively. The peak observed at $m/z = 1026.09$ is due to loss of one chlorine atom. The peak at $m/z = 911.11$ is due to the loss of second chlorine atom. Several other fragments at $m/z = 898.00$, 729.04 , 696.05 , 661.06 , 626.02 , 466.91 , 365.02 , and 262.08 are observed, which are attributed to fragments associated with complex and proposed fragmentation pattern of complex **1** is shown in Supplementary Material. In the mass spectrum of complex **7**, molecular ion peak at $m/z = 837.96$, 839.99 , 841.93 , 843.92 , and 845.90 are assigned as (M^+), ($M + 2$), ($M + 4$), ($M + 6$), and ($M + 8$) peaks due to the presence of four chlorine atoms. The peak observed at $m/z = 799.00$ is due to loss of one chlorine atom. The peak at $m/z = 470.89$ is due to the loss of neutral bidentate ligand. Several other fragments at $m/z = 764.09$, 729.02 , 466.93 , 436.00 , 398.90 , 365.07 , 364.01 and 262.10 are observed, which attributed to fragments associated with complex. Proposed fragmentation pattern for the complex **7** is shown in Supplementary Material.

In vitro antibacterial activity

The interpretation of antimicrobial potency is carried out in terms minimum inhibitory concentration (MIC) defined as the lowest concentration, which inhibits the growth of microorganism, referred by lack of turbidity in the tube. If for a specific concentration of the test compounds no turbidity is observed, then a whole experimental procedure is repeated with the next dilution i.e. half the concentration of test compound that was previously added. This procedure is repeated until the faint turbidity by the inoculums itself is observed and the said concentration is termed as MIC. The result of MIC in terms of μM is represented in Table 1. The result of antibacterial activity indicates that the synthesized complexes are more potent than the reference ligands but the complexes are less potent as compared to

the standard antibiotics like ciprofloxacin and ofloxacin. The mechanism of toxicity of the complexes may be ascribed to the increase of the lipophilic nature of the complexes arising from chelation. The mode of action of antimicrobials may involve different targets in pathogens, e.g. interference with cell wall synthesis and damage to the cytoplasmic membrane, as a result of which cell permeability may be altered leading to cell death. Another mechanism of toxicity of these complexes to microorganisms may be due to the inhibition of energy production or ATP production, by inhibiting respiration or by the uncoupling of oxidative phosphorylation. The increase in antimicrobial activity of metal complexes can be the result of: (I) chelate effects, (II) nature of the ligands, (III) total charge of the complex, (IV) nature of the ion neutralising the complex, and (V) nuclearity of the metal centre in the compounds. The inhibition activity seems to be governed in certain degree by the facility of coordination at the metal centre as well as electronic nature of the ligands (Figs. 1, 2).

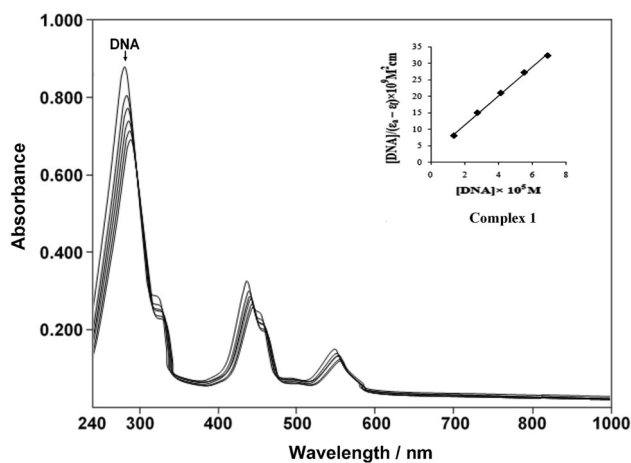
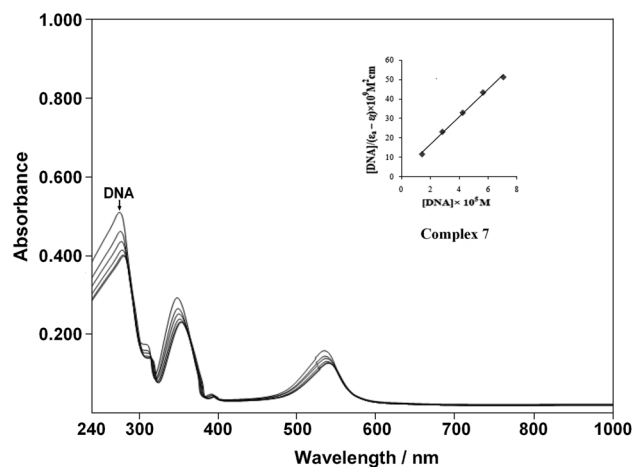
DNA binding mode investigation

Quantitative binding strength of the complex was carried out by absorption titration method. In the intercalation mode of binding of metal complex with DNA, there is an interaction of π^* orbital of the intercalated ligand which may couple with the π orbital of the DNA base pairs, resulting in the lowering of $\pi-\pi^*$ transition energy and thus displays a red shift in the transition [16]. On the other hand, hypochromism is observed when there is a coupling of a π orbital with partially filled electrons [17]. The overlay spectrum of complex **1** and **7** are represented in Figs. 3 and 4, respectively. In the overlay spectrum of complex **1** and **7**, hypochromism and red shift are observed, which suggest the intercalation mode of binding. The intrinsic binding constant values (K_b) for the synthesized complexes are represented in the Table 2. The K_b values for the synthesized complexes are found in the range of 0.521×10^5 – $2.94 \times 10^5 \text{ M}^{-1}$, which are higher than $\Delta\Delta - \{[\text{Ru}(\text{Me}_2\text{bpy})_2]_2(\mu\text{-bpm})\}^{4+}$ (1×10^3) [18], while the obtained K_b values are lower as compared to the $[\text{Ru}(\text{bpy})_2(\text{dppz})]^{2+}$ ($>10^6$) [19]. The difference in the K_b value of the synthesized complexes is attributed to their relative hydrophobic character of the ligands which is affected by the substituent present in the ligands [20]. To further confirm the binding mode of the complexes, viscosity measurements were carried out. The viscosity titration curve of the ruthenium complexes **1–12** are represented in Fig. 3.

The figure shows that successive addition of ruthenium complexes to the solution of herring sperm (HS-) DNA increases its relative viscosity, suggesting classical intercalation mode of binding as hypochromism with red shift is

Table 1 MIC values of synthesized ligands L¹–L⁶ and complexes 1–12

Sr. no.	MIC values				
	Gram-positive		Gram-negative		
	<i>S. Aureus</i>	<i>B. subtilis</i>	<i>S. marcescens</i>	<i>P. aeruginosa</i>	<i>E. coli</i>
L ¹	265	255	230	300	190
L ²	245	280	260	350	255
L ³	280	275	290	450	215
L ⁴	235	265	280	345	210
L ⁵	270	255	265	390	240
L ⁶	250	240	325	470	225
1	155	210	160	170	145
2	190	210	180	165	165
3	200	260	210	225	190
4	170	230	180	185	175
5	210	235	180	200	200
6	235	245	220	225	210
7	125	130	120	120	115
8	160	140	140	145	125
9	175	190	175	160	150
10	135	160	150	155	120
11	165	165	150	170	140
12	170	210	180	185	190

**Fig. 1** Electronic absorption spectra of complex 1 with increasing concentration of herring sperm DNA (HS-DNA) in phosphate buffer. Inset plots of $[DNA]/(\epsilon_a - \epsilon_p)$ versus $[DNA]$ for the titration of DNA with ruthenium(III) complexes**Fig. 2** Electronic absorption spectra of complex 7 with increasing concentration of herring sperm DNA (HS-DNA) in phosphate buffer. Inset plots of $[DNA]/(\epsilon_a - \epsilon_p)$ versus $[DNA]$ for the titration of DNA with ruthenium(III) complexes

observed in absorption titration measurement. If blue shift was observed in absorption titration, the interaction mode of complexes with DNA will be the partial intercalation. Ruthenium complexes interact with DNA by incorporation of planar aromatic ligand into DNA base pairs, hence

leading to the increase of the relative specific viscosity of DNA. The conclusion is in agreement with absorption titration method. Similar results were reported for the ethidium bromide (EB) and $[Ru(\text{phen})_2(\text{MIP})](\text{ClO}_4)_2 \cdot 2.5\text{H}_2\text{O}$ [21].

Fig. 3 Effect on relative viscosity of HS-DNA under the influence of increasing amount of complexes at 37 ± 1 °C in phosphate buffer ($\text{Na}_2\text{HPO}_4/\text{NaH}_2\text{PO}_4$, pH 7.2)

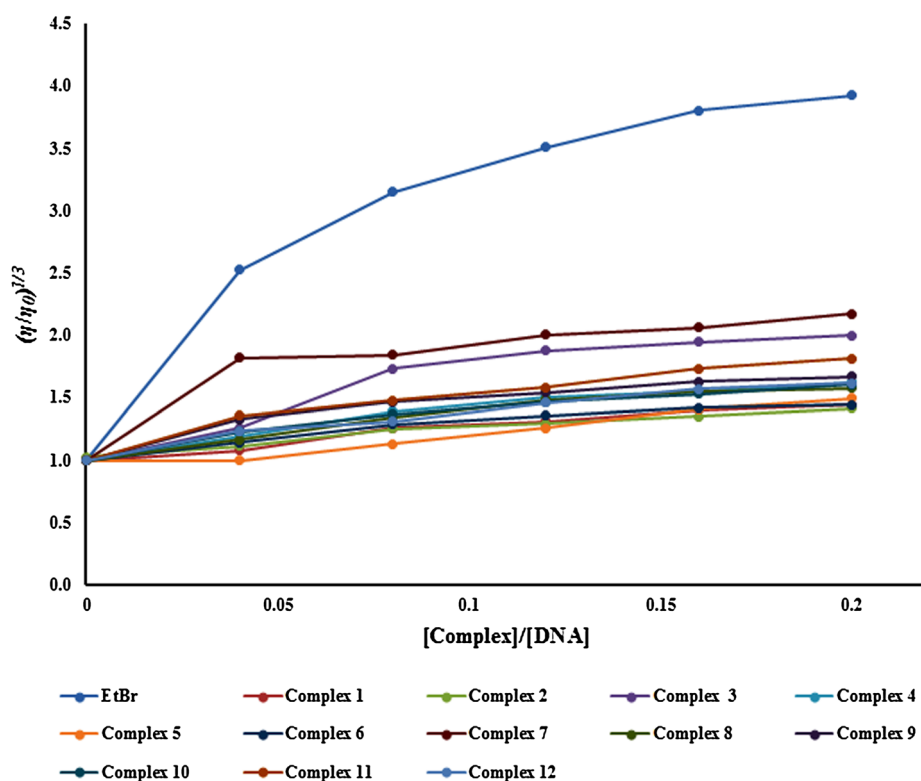


Fig. 4 Average % mortality of brine shrimp against increasing amount of complex concentration

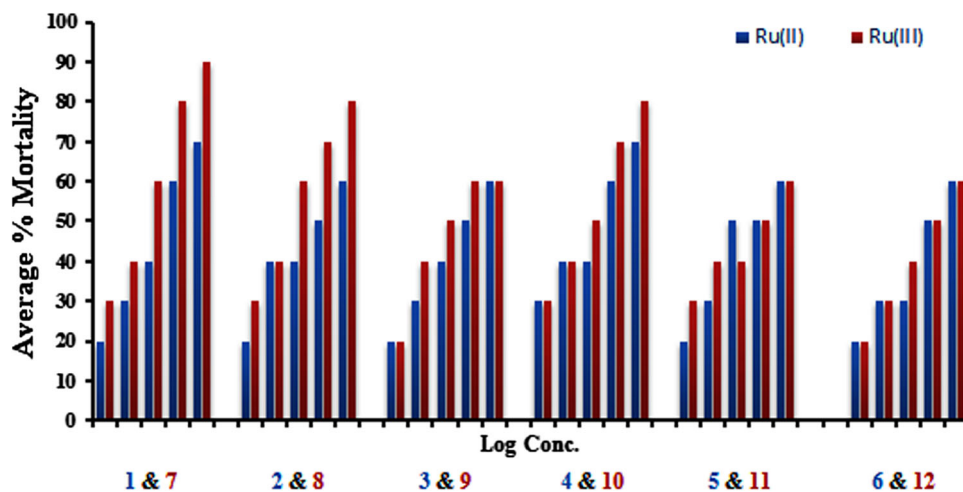
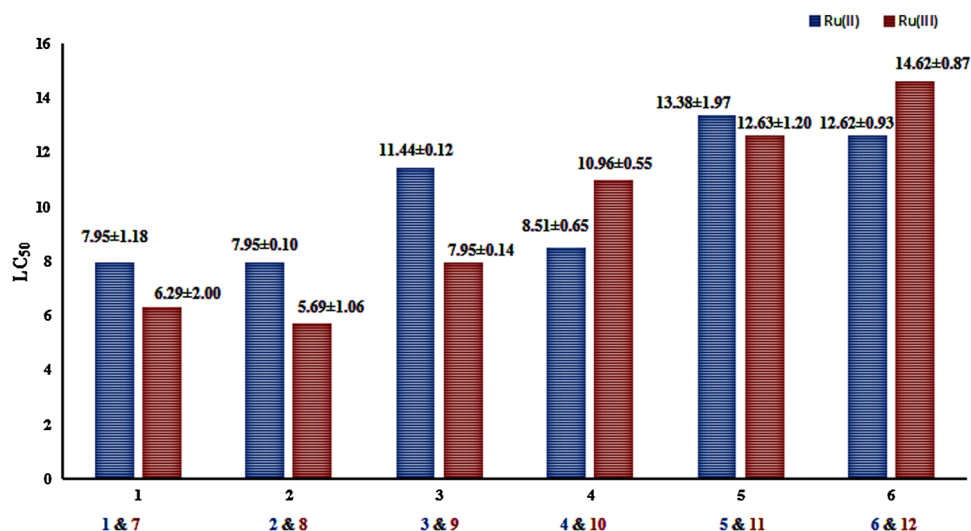
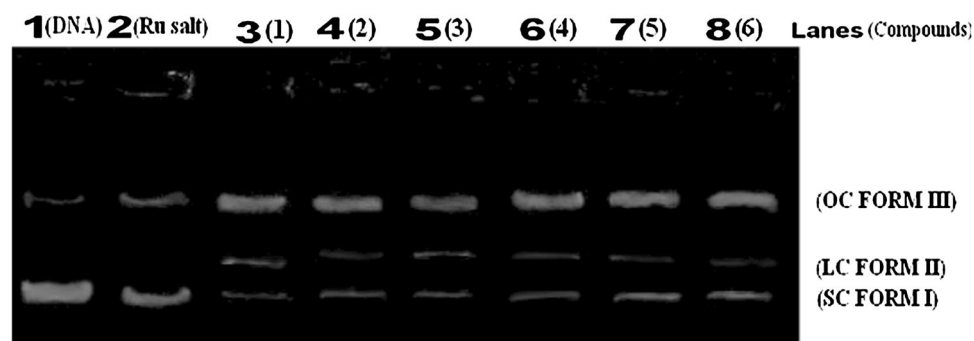


Table 2 Intrinsic binding constant (K_b) values of the complex

Complexes	$K_b \times 10^5 \text{ M}^{-1}$	Complexes	$K_b \times 10^5 \text{ M}^{-1}$
1	1.74	7	2.94
2	1.23	8	1.86
3	1.42	9	1.41
4	0.759	10	1.40
5	0.521	11	1.29
6	0.585	12	1.49

Brine shrimp lethality bioassay: a cytotoxicity profile

All test tubes were incubated for 24 h at room temperature. Number of dead nauplii is counted after 24 and 48 h. With the help of magnifying glass. The percentage mortality of brine shrimp nauplii was determined from the number of dead nauplii. And the LC_{50} was calculated from the plot of log of concentration of samples plotted against percent of mortality of nauplii. From the result represented in Figs. 4

Fig. 5 LC₅₀ value of the complexes**Fig. 6** Cleavage of pUC19 plasmid DNA under the influence of ruthenium(II) complexes. Lane 1 DNA control, lane 2 RuCl₃·3H₂O, lane 3 [Ru(L¹)(PPh₃)₂Cl₂] (1), lane 4 [Ru(L²)(PPh₃)₂Cl₂] (2), lane 5 [Ru(L³)(PPh₃)₂Cl₂] (3), lane 6 [Ru(L⁴)(PPh₃)₂Cl₂] (4), lane 7 [Ru(L⁵)(PPh₃)₂Cl₂] (5), lane 8 [Ru(L⁶)(PPh₃)₂Cl₂] (6)

and 5, it is inferred that % mortality of brine shrimp found to increase with increase in the concentration of complexes and the complexes of ruthenium(III) exhibit higher toxicity at lower concentration than other synthesized ruthenium(II) complexes, suggesting its low concentration effects the growth of *Artemia* cysts. However, the LC₅₀ of synthesized complexes (LC₅₀ = 5.69 ± 1.06–14.62 ± 0.87 μg cm⁻³) are comparable to standard anticancer agent cisplatin (LC₅₀ < 4 μg cm⁻³).

Photochemical investigation of DNA nuclease activity

Figures 6 and 7 show the cleavage of pUC19 DNA by ruthenium(II) and ruthenium(III) complexes respectively, along with reference standard RuCl₃·3H₂O. The difference was observed in the bands of RuCl₃·3H₂O (lane 2) and complexes (lanes 3–8) compared with the control DNA (lane 1). Control DNA shows only two bands corresponding to supercoiled form (form I) and circular form (form III). Lane 2 (RuCl₃·3H₂O + DNA) also show two bands but intensity of supercoiled form is different from that of control. Lane 3–8

(complexes + DNA) shows three bands, an additional linear form (form II) indicating a significant cleavage of DNA by the test complexes in reference to parent compound RuCl₃·3H₂O. Quantitative measure of the DNA cleavage in terms of % cleavage for the test compounds are represented in the Table 3. As the complexes are observed to cleave the DNA, it is concluded that the complexes control the growth of the microorganisms by cleaving the DNA.

Conclusion

Synthesized blackish-brown Ru(II) complexes are unstable in air and diamagnetic while reddish-brown Ru(III) complexes are stable in air. Electronic spectra support the ruthenium ion in an octahedron geometry. It is found that experimental percentage for C, H, and N atom in the complex matches well with the theoretical values for the proposed structure. The proof for the proposed structure has also been strengthened from molecular ion peak in the mass spectrum analysis and from the decomposition of fragments occurring in TGA analysis at different

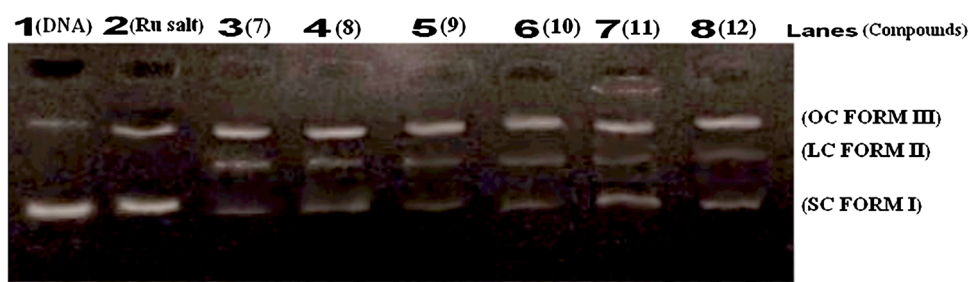


Fig. 7 Cleavage of pUC19 plasmid DNA under the influence of ruthenium(III) complexes. Lane 1 DNA control, lane 2 $\text{RuCl}_3 \cdot 3\text{H}_2\text{O}$, lane 3 $[\text{Ru}(\text{L}^1)(\text{PPh}_3)\text{Cl}_3]$ (7), lane 4 $[\text{Ru}(\text{L}^2)(\text{PPh}_3)\text{Cl}_3]$ (8), lane 5

$[\text{Ru}(\text{L}^3)(\text{PPh}_3)\text{Cl}_3]$ (9), lane 6 $[\text{Ru}(\text{L}^4)(\text{PPh}_3)\text{Cl}_3]$ (10), lane 7 $[\text{Ru}(\text{L}^5)(\text{PPh}_3)\text{Cl}_3]$ (11), lane 8 $[\text{Ru}(\text{L}^6)(\text{PPh}_3)\text{Cl}_3]$ (12)

Table 3 Complexes mediated cleavage data of pUC19 DNA

Compounds	% SC	% OC	% LC	% Cleavage
<i>Gel-1</i>				
Control	86.8	13.2	–	–
$\text{RuCl}_3 \cdot 3\text{H}_2\text{O}$	67.1	32.9	–	22.69
$[\text{Ru}(\text{PPh}_3)_2(\text{L}^1)\text{Cl}_2]$ (1)	9.5	68.5	22.5	89.05
$[\text{Ru}(\text{PPh}_3)_2(\text{L}^2)\text{Cl}_2]$ (2)	11.6	68.1	20.3	86.63
$[\text{Ru}(\text{PPh}_3)_2(\text{L}^3)\text{Cl}_2]$ (3)	15.8	77.1	7.4	81.79
$[\text{Ru}(\text{PPh}_3)_2(\text{L}^4)\text{Cl}_2]$ (4)	12.7	76.5	16.9	85.36
$[\text{Ru}(\text{PPh}_3)_2(\text{L}^5)\text{Cl}_2]$ (5)	24.3	62.2	13.4	72.00
$[\text{Ru}(\text{PPh}_3)_2(\text{L}^6)\text{Cl}_2]$ (6)	12.1	72.8	15.0	86.05
<i>Gel-2</i>				
Control	83.1	16.9	–	–
$\text{RuCl}_3 \cdot 3\text{H}_2\text{O}$	66.1	33.9	–	20.45
$[\text{Ru}(\text{PPh}_3)(\text{L}^1)\text{Cl}_3]$ (7)	11.6	60.1	28.3	86.04
$[\text{Ru}(\text{PPh}_3)(\text{L}^2)\text{Cl}_3]$ (8)	12.4	66.9	18.4	85.07
$[\text{Ru}(\text{PPh}_3)(\text{L}^3)\text{Cl}_3]$ (9)	19.6	64.2	16.1	76.41
$[\text{Ru}(\text{PPh}_3)(\text{L}^4)\text{Cl}_3]$ (10)	21.6	63.9	14.5	74.00
$[\text{Ru}(\text{PPh}_3)(\text{L}^5)\text{Cl}_3]$ (11)	29.4	57.9	12.7	64.62
$[\text{Ru}(\text{PPh}_3)(\text{L}^6)\text{Cl}_3]$ (12)	26.3	60.1	18.6	68.35

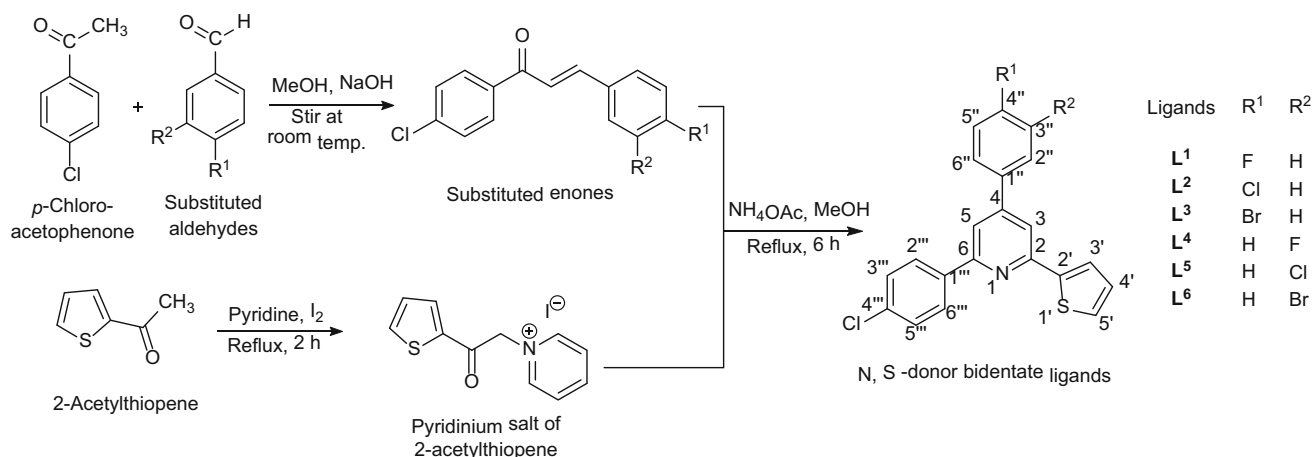
temperature range supporting the theoretically proposed structure of complex. The increase in the antimicrobial potency of the complexes as compared to ligands is attributed to the chelate effect which increases lipophilicity of complexes. Complex 7 showed higher potency towards all the bacterial strains compared to other test compounds. All the synthesized ruthenium complexes bind in an intercalative mode of binding action and the quantitative binding strength of ruthenium(III) complexes are found higher than ruthenium(II) complexes. Cytotoxicity studies of metal complexes shows good potency against brine shrimp and 100 % mortality is achieved after 48 h of incubation. LC_{50} values of ruthenium(III) complexes are found to lower compared to ruthenium(II) complexes with similar ligands, indicating significantly high toxicity of ruthenium(III) complexes as compared to ruthenium(II) complexes. LC_{50} values of the complexes are found to be

lower as compared to potassium dichromate suggesting that complexes are significantly toxic at low concentration and their lower dose can inhibit the 50 % of population of test species as compared to the higher dose required for the potassium dichromate and can be further explored for in vivo cytotoxicity studies against cell lines. Highly efficient cleavage of supercoiled pUC19 DNA is observed for all the complexes compared to the metal salt.

Experimental

All the chemicals purchased were of analytical grade and used as such without further purification. Ruthenium trichloride trihydrate, 2-acetylthiophene, 3-chlorobenzaldehyde, 3-fluorobenzaldehyde, 3-bromobenzaldehyde, 4-chlorobenzaldehyde, 4-fluorobenzaldehyde,

Scheme 1



4-bromobenzaldehyde, and HS-DNA were purchased from Sigma Chemical Co. (India). Ethidium bromide (EB), bromophenol blue, agarose, and Luria Broth (LB) were purchased from Himedia (India). Culture of pUC19 bacteria (MTCC 47) was purchased from Institute of Microbial Technology (Chandigarh, India).

A Perkin-Elmer 240 Elemental Analyser was used to collect microanalytical data (C, H, N). Room temperature magnetic susceptibility was measured by Gouy's method using mercury tetrathiocyanatocobaltate(II) as the calibrant ($\chi_g = 16.44 \times 10^{-6}$ cgs units at 20 °C), on Citizen Balance. The diamagnetic correction has been made using Pascal's constant. FT-IR data were collected with the help of FT-IR ABB Bomen MB 3000 spectrophotometer. UV-Vis spectra of the complex were recorded on UV-160A UV-Vis spectrophotometer, Shimadzu (Japan) and corrected for background due to solvent absorption. The percentage of pUC19 DNA cleavage was quantified by AlphaDigiDoc™ RT. Version V.4.0.0 PC-Image software.

2-(4-Chlorophenyl)-4-(4-fluorophenyl)-6-(thiophen-2-yl)pyridine (L¹, C₂₁H₁₃ClFNS)

Modified Krohnke pyridine synthesis was used for the synthesis of ligands [22]. Enone synthesized by the reaction between *p*-fluorobenzaldehyde and *p*-chloroacetophenone, was refluxed with pyridinium salt of 2-acetylthiophene in presence of ammonium acetate for 6 h. The reaction mixture was allowed to cool at room temperature. The solid product was filtered and recrystallized from hexane. General reaction scheme for the synthesis of ligands is shown in Scheme 1. Yield 65 %; m.p.: 138 °C; ¹H NMR (400 MHz, CDCl₃, Me₄Si): $\delta = 8.14$ – 8.11 (2H, m, H_{3,5}), 7.74 – 7.69 (5H, m, H_{5',2'',3'',5'',6''}), 7.51 – 7.46 (3H, m, H_{3',3'',5''}), 7.26 – 7.22 (2H, m, H_{2',6''}), 7.19 – 7.16 (1H, m, H_{4'}) ppm; ¹³C NMR (100 MHz,

CDCl₃, Me₄Si): $\delta = 164.75$ (C_{4'''}), 156.16 (C₂), 152.93 (C₆), 149.32 (C_{2'}), 145.09 (C_{1'''}), 137.34 (C_{1''}), 134.76 (C_{6'''}), 134.73 (C_{2'''}), 128.94 (C_{5'}), 128.91 (C_{3'}), 128.86 (C_{4'}), 128.30 (C_{5''}), 128.03 (C_{3''}), 127.93 (C_{6''}), 124.85 (C_{2''}), 116.07 ppm; IR: $\bar{\nu} = 3066$ ν (C–H)_{ar}, 1545 ν (C=C), 1397 ν (C=N), 1179 ν (C=S), 1229 ν (C–F), 1092 ν (C–Cl), 1381, 1362 pyridine skeleton band, 800 ν (C–H), 1112, 826 (*p*-substituted ring) cm⁻¹.

2,4-Bis(4-chlorophenyl)-6-(thiophen-2-yl)pyridine (L², C₂₁H₁₃Cl₂NS)

It has been synthesized by the reaction between pyridinium salt of 2-acetylthiophene and enone of *p*-chlorobenzaldehyde and *p*-chloroacetophenone. Yield 60 %; m.p.: 140 °C; ¹H NMR (400 MHz, CDCl₃, Me₄Si): $\delta = 8.13$ (2H, d, H_{3,5}), 7.75 (3H, d, H_{5',3'',5''}), 7.68 (2H, d, H_{2'',6''}), 7.54–7.46 (5H, m, H_{3',2',3'',5'',6''}), 7.18 (1H, dd, H_{4'}) ppm; ¹³C NMR (100 MHz, CDCl₃, Me₄Si): $\delta = 156.28$ (C₆), 153.03 (C₂), 151.26 (C₄), 149.13 (C_{2'}), 145.02 (C_{1'''}), 137.31 (C_{1''}), 137.09 (C_{4'''}), 135.44 (C_{4''}), 129.38 (C_{3',5''}), 128.94 (C_{3'',5''}), 128.40 (C_{2',6''}), 128.29 (C_{2'',6''}), 128.06 (C_{5'}), 127.98 (C_{4'}), 124.89 (C_{3'}), 116.21 (C₃), 115.26 (C₅) ppm; IR: $\bar{\nu} = 3061$ ν (C–H)_{ar}, 1546 ν (C=C), 1397 ν (C=N), 1176 ν (C=S), 1082 ν (C–Cl), 1383, 1304 pyridine skeleton band, 778 ν (C–H), 1123, 830 (*p*-substituted ring) cm⁻¹.

4-(4-Bromophenyl)-2-(4-chlorophenyl)-6-(thiophen-2-yl)pyridine (L³, C₂₁H₁₃ClBrNS)

It has been synthesized by the reaction between pyridinium salt of 2-acetylthiophene and enone of *p*-bromobenzaldehyde and *p*-chloroacetophenone. Yield 62 %; m.p.: 123 °C; ¹H NMR (400 MHz, CDCl₃, Me₄Si): $\delta = 8.12$ (2H, d, H_{3,5}), 7.73 (3H, t, H_{5',3'',5''}), 7.68 (2H, d, H_{2'',6''}), 7.60 (2H, d, H_{2',6''}), 7.48 (3H, dd, H_{3',3'',5''}), 7.18 (1H, t, H_{4'}) ppm; ¹³C NMR (100 MHz, CDCl₃, Me₄Si): $\delta = 156.29$ (C₆), 153.92 (C₂), 153.07 (C₄), 149.19 (C_{2'}),

145.00 (C_{1'''}), 137.54 (C_{1''}), 137.26 (C_{4'''}), 135.46 (C_{4''}), 132.34 (C_{3'''},_{5'''}), 128.93 (C_{3''},_{5''}), 128.68 (C_{2''},_{6''}), 128.29 (C_{2'''},_{6'''}), 128.04 (C_{5'}), 128.00 (C_{4'}), 124.92 (C_{3'}), 116.12 (C₃), 115.17 (C₅) ppm; IR: $\bar{\nu}$ = 3052 ν (C–H)_{ar}, 1545 ν (C=C), 1390 ν (C=N), 1170 ν (C=S), 1095 ν (C–Cl), 1012 ν (C–Br), 1380, 1360 pyridine skeleton band, 750 ν (C–H), 1150, 815 (*p*-substituted ring) cm⁻¹.

2-(4-Chlorophenyl)-4-(3-fluorophenyl)-6-(thiophen-2-yl)pyridine (**L**⁴, C₂₁H₁₃ClFNS)

It has been synthesized using the chalcone prepared from the reaction between *m*-fluorobenzaldehyde and *p*-chloroacetophenone. Yield 69 %; m.p.: 118 °C; ¹H NMR (400 MHz, CDCl₃, Me₄Si): δ = 8.35–8.32 (2H, dd, H_{2'''},_{6'''}), 8.26–8.20 (2H, dd, H_{3'''},_{5'''}), 8.14–8.09 (1H, dd, H₃), 7.99–7.91 (2H, m, H_{3'},_{5'}), 7.71–7.69 (1H, dd, H₅), 7.63–7.61 (3H, dd, H_{2''},_{4''},_{6''}), 7.42–7.34 (1H, t, H_{5''}), 7.30–7.22 (1H, dd, H_{4'}) ppm; ¹³C NMR (100 MHz, CDCl₃, Me₄Si): δ = 158.68 (C_{3''}), 155.78 (C₆), 149.83 (C₂), 148.23 (C₄), 143.07 (C_{1''}), 141.85 (C_{2'}), 139.12 (C_{1'''}), 136.52 (C_{4'''}), 131.23 (C_{5'}), 129.91 (C_{3'''}, C_{5'''}), 128.71 (C_{2'''},_{6'''}), 127.55 (C_{3'},_{4'},_{5'}), 123.5 (C_{6''}), 116.70 (C₃), 115.11 (C_{4''}), 112.14 (C_{2''}), 108.90 (C₅) ppm; IR: $\bar{\nu}$ = 3066 ν (C–H)_{ar}, 1546 ν (C=C), 1398 ν (C=N), 1157 ν (C=S), 1225 ν (C–F), 1092 ν (C–Cl), 1363 pyridine skeleton band, 788, 826 (*m*-substituted ring) cm⁻¹.

4-(3-Chlorophenyl)-2-(4-chlorophenyl)-6-(thiophen-2-yl)pyridine (**L**⁵, C₂₁H₁₃Cl₂NS)

It has been synthesized using the chalcone prepared from the reaction between *m*-chlorobenzaldehyde and *p*-chloroacetophenone. Yield 58 %; m.p.: 109 °C; ¹H NMR (400 MHz, CDCl₃, Me₄Si): δ = 8.16–8.14 (3H, d, H_{3,2'''},_{6'''}), 7.84 (1H, s, H₅), 7.52–7.752 (2H, m, H_{3''},_{5''}), 7.51–7.50 (1H, t, H_{5''}), 7.50–7.48 (6H, m, H_{3',4',5',2'',4'',6''}) ppm; ¹³C NMR (100 MHz, CDCl₃, Me₄Si): δ = 157.10 (C_{3''}), 154.20 (C₆), 150.33 (C₂), 143.44 (C_{4'}), 138.16 (C_{1''}, C_{2'}), 136.52 (C_{1'''},_{4'''}), 132.56 (C_{3'''},_{5'''}), 130.13 (C_{2'''},_{6'''}), 128.25 (C_{3'},_{4'},_{5'}), 126.12 (C_{3,5''},_{6''}), 123.57 (C_{4''}), 116.54 (C_{2''}), 115.45 (C₅) ppm; IR: $\bar{\nu}$ = 3067 ν (C–H)_{ar}, 1548 ν (C=C), 1396 ν (C=N), 1158 ν (C=S), 1182 ν (C–Cl), 1354 pyridine skeleton band, 785, 826 (*m*-substituted ring) cm⁻¹.

4-(3-Bromophenyl)-2-(4-chlorophenyl)-6-(thiophen-2-yl)pyridine (**L**⁶, C₂₁H₁₃BrClNS)

It has been synthesized using the chalcone prepared from the reaction between *m*-bromobenzaldehyde and *p*-chloroacetophenone. Yield 52 %; m.p.: 90 °C; ¹H NMR (400 MHz, CDCl₃, Me₄Si): δ = 8.15–8.11 (2H, d, H_{2'''},_{6'''}), 7.96–7.97 (1H, d, H₃), 7.80–7.60 (4H, m, H_{2'',4'',3'',5''}), 7.58–7.41 (5H, m, H_{5,3',5',5',6''}), 7.18–7.16 (1H, d, H_{4'}) ppm; ¹³C NMR (100 MHz, CDCl₃, Me₄Si): δ = 158.12 (C_{3''}), 154.58 (C₆), 149.03 (C₂), 143.02 (C₄), 139.19 (C_{1''}), 137.34 (C_{2'}), 130.73 (C_{1'''},_{4'''}), 128.52 (C_{5'}),

126.62 (C_{3'''},_{5'''}), 122.83 (C_{2'''},_{6'''}), 120.43 (C_{4'}), 118.14 (C_{5''},_{6''}), 116.50 (C_{3'}), 115.07 (C_{2''},_{4''}), 112.52 (C₃), 109.12 (C₅) ppm; IR: $\bar{\nu}$ = 3055 ν (C–H)_{ar}, 1548 ν (C=C), 1393 ν (C=N), 1154 ν (C=S), 1180 ν (C–Cl), 1008 ν (C–Br) 1354 pyridine skeleton band, 789, 821(*m*-substituted ring) cm⁻¹.

Synthesis of complexes

A ruthenium precursor [RuCl₃(PPh₃)₃] was prepared by the refluxing the methanolic solution of RuCl₃·3H₂O and PPh₃ (1:3) in presence of conc. HCl for 1 h. The reddish brown precipitate obtained was filtered, dried and recrystallized from hot methanol.

Dichloro[2-(4-chlorophenyl)-4-(4-fluorophenyl)-6-(thiophen-2-yl)pyridine]bis(triphenylphosphine)ruthenium(II) [RuCl₂(PPh₃)₂L¹] (**1**, C₅₇H₄₃Cl₃FNP₂RuS)

It has been synthesized by refluxing the solution of ruthenium precursor [RuCl₃(PPh₃)₃] in toluene (0.1 mmol) with the methanolic solution of 2-(4-chlorophenyl)-4-(4-fluorophenyl)-6-(thiophen-2-yl)pyridine (**L**¹, 0.1 mmol) in presence of Et₃N as a reducing agent (0.1 mmol in methanol) and LiCl (0.4 mmol in methanol) (to prevent excessive loss of Cl from the synthesized precursor) for 4 h (Scheme 2) [23, 24]. The resulting solution has been concentrated to half of its volume and the product has been separated by adding small amount of pet ether (60:80). The obtained blackish brown product was washed with methanol and dried under vacuum. Yield 15.0 %; m.p.: 244.1 °C; UV–Vis (DMSO): λ_{\max} = 550, 440, 273 nm.

Dichloro[2,4-bis(4-chlorophenyl)-6-(thiophen-2-yl)pyridine]bis(triphenylphosphine)ruthenium(II) [RuCl₂(PPh₃)₂L²] (**2**, C₅₇H₄₃Cl₄NP₂RuS)

It has been synthesized using [RuCl₃(PPh₃)₃] and 2,4-bis(4-chlorophenyl)-6-(thiophen-2-yl)pyridine (**L**²). Yield 15.9 %; m.p.: 253.0 °C; UV–Vis (DMSO): λ_{\max} = 554, 440, 263 nm.

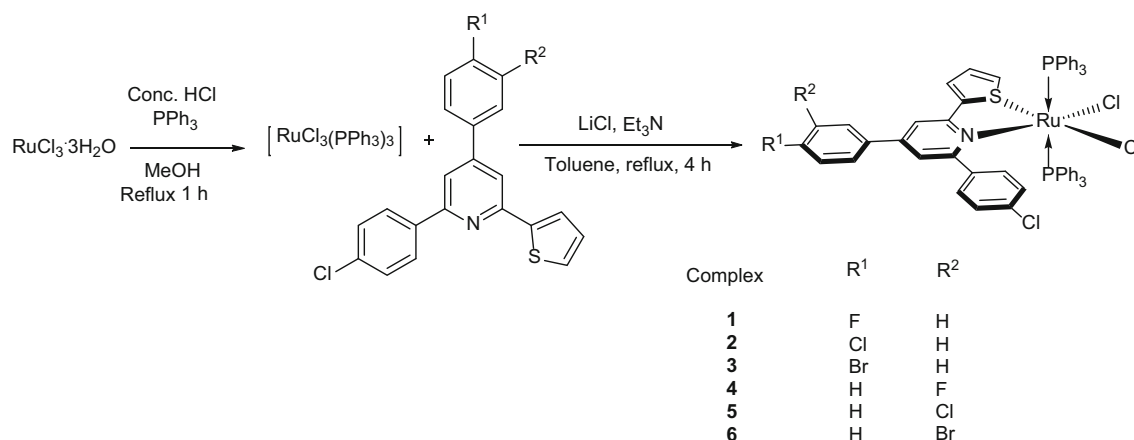
Dichloro[4-(4-bromophenyl)-2-(4-chlorophenyl)-6-(thiophen-2-yl)pyridine]bis(triphenylphosphine)ruthenium(II) [RuCl₂(PPh₃)₂L³] (**3**, C₅₇H₄₃BrCl₃NP₂RuS)

It has been synthesized using [RuCl₃(PPh₃)₃] and 4-(4-bromophenyl)-2-(4-chlorophenyl)-6-(thiophen-2-yl)pyridine (**L**³). Yield 17.2 %; m.p.: 234.7 °C; UV–Vis (DMSO): λ_{\max} = 557, 431, 262 nm.

Dichloro[2-(4-chlorophenyl)-4-(3-fluorophenyl)-6-(thiophen-2-yl)pyridine]bis(triphenylphosphine)ruthenium(II) [RuCl₂(PPh₃)₂L⁴] (**4**, C₅₇H₄₃Cl₃FNP₂RuS)

It has been synthesized using [RuCl₃(PPh₃)₃] and 2-(4-chlorophenyl)-4-(3-fluorophenyl)-6-(thiophen-2-yl)pyridine (**L**⁴). Yield 16.9 %; m.p.: 247.5 °C; UV–Vis (DMSO): λ_{\max} = 560, 426, 269 nm.

Scheme 2



Dichloro[4-(3-chlorophenyl)-2-(4-chlorophenyl)-6-(thiophen-2-yl)pyridine]bis(triphenylphosphine)ruthenium(II) [$\text{RuCl}_2(\text{PPh}_3)_2\text{L}^5$] (**5**, $\text{C}_{57}\text{H}_{43}\text{Cl}_4\text{NP}_2\text{RuS}$)

It has been synthesized using $[\text{RuCl}_3(\text{PPh}_3)_3]$ and 4-(3-chlorophenyl)-2-(4-chlorophenyl)-6-(thiophen-2-yl)pyridine (**L**⁵). Yield 15.2 %; m.p.: 256.8 °C; UV–Vis (DMSO): $\lambda_{\text{max}} = 568, 422, 265 \text{ nm}$.

Dichloro[4-(3-bromophenyl)-2-(4-chlorophenyl)-6-(thiophen-2-yl)pyridine]bis(triphenylphosphine)ruthenium(II) [$\text{RuCl}_2(\text{PPh}_3)_2\text{L}^6$] (**6**, $\text{C}_{57}\text{H}_{43}\text{BrCl}_3\text{NP}_2\text{RuS}$)

It has been synthesized using the $[\text{RuCl}_3(\text{PPh}_3)_3]$ and 4-(3-bromophenyl)-2-(4-chlorophenyl)-6-(thiophen-2-yl)pyridine (**L**⁶). Yield 14.8 %; m.p.: 272.0 °C; UV–Vis (DMSO): $\lambda_{\text{max}} = 560, 420, 263 \text{ nm}$.

Trichloro[2-(4-chlorophenyl)-4-(4-fluorophenyl)-6-(thiophen-2-yl)pyridine](triphenylphosphine)ruthenium(III) [$\text{RuCl}_3(\text{PPh}_3)\text{L}^1$] (**7**, $\text{C}_{39}\text{H}_{28}\text{Cl}_4\text{FNPRuS}$)

It has been synthesized by refluxing the solution of ruthenium precursor $[\text{RuCl}_3(\text{PPh}_3)_3]$ in toluene (0.1 mmol) with the methanolic solution of 2-(4-chlorophenyl)-4-(4-fluorophenyl)-6-(thiophen-2-yl)pyridine (**L**¹, 0.1 mmol) for 4 h (Scheme 3). The resulting solution has been concentrated to half of its volume and the product was separated by adding small amount of pet ether (60:80). The blackish brown product obtained was washed with methanol, toluene, and finally dried under vacuum. Yield 17 %; m.p.: 249 °C; $\mu_{\text{eff}} = 1.92 \text{ B.M.}$; UV–Vis (DMSO): $\lambda_{\text{max}} = 540, 385, 270 \text{ nm}$.

Trichloro[2,4-bis(4-chlorophenyl)-6-(thiophen-2-yl)pyridine](triphenylphosphine)ruthenium(III) [$\text{RuCl}_3(\text{PPh}_3)\text{L}^2$] (**8**, $\text{C}_{39}\text{H}_{28}\text{Cl}_5\text{NPRuS}$)

It has been synthesized using $[\text{RuCl}_3(\text{PPh}_3)_3]$ and 2,4-bis(4-chlorophenyl)-6-(thiophen-2-yl)pyridine (**L**²). Yield 20 %; m.p.: 255 °C; $\mu_{\text{eff}} = 1.89 \text{ B.M.}$; UV–Vis (DMSO): $\lambda_{\text{max}} = 562, 362, 272 \text{ nm}$.

Trichloro[4-(4-bromophenyl)-2-(4-chlorophenyl)-6-(thiophen-2-yl)pyridine](triphenylphosphine)ruthenium(III) [$\text{RuCl}_3(\text{PPh}_3)\text{L}^3$] (**9**, $\text{C}_{39}\text{H}_{28}\text{BrCl}_4\text{NPRuS}$)

It has been synthesized using $[\text{RuCl}_3(\text{PPh}_3)_3]$ and 4-(4-bromophenyl)-2-(4-chlorophenyl)-6-(thiophen-2-yl)pyridine (**L**³). Yield 17 %; m.p.: 288 °C; $\mu_{\text{eff}} = 1.84 \text{ B.M.}$; UV–Vis (DMSO): $\lambda_{\text{max}} = 560, 369, 272 \text{ nm}$.

Trichloro[2-(4-chlorophenyl)-4-(3-fluorophenyl)-6-(thiophen-2-yl)pyridine](triphenylphosphine)ruthenium(III) [$\text{RuCl}_3(\text{PPh}_3)\text{L}^4$] (**10**, $\text{C}_{39}\text{H}_{28}\text{Cl}_4\text{FNPRuS}$)

It has been synthesized using $[\text{RuCl}_3(\text{PPh}_3)_3]$ and 2-(4-chlorophenyl)-4-(3-fluorophenyl)-6-(thiophen-2-yl)pyridine (**L**⁴). Yield 18 %; m.p.: 275 °C; $\mu_{\text{eff}} = 1.79 \text{ B.M.}$; UV–Vis (DMSO): $\lambda_{\text{max}} = 544, 358, 270 \text{ nm}$.

Trichloro[4-(3-chlorophenyl)-2-(4-chlorophenyl)-6-(thiophen-2-yl)pyridine](triphenylphosphine)ruthenium(III) [$\text{RuCl}_3(\text{PPh}_3)\text{L}^5$] (**11**, $\text{C}_{39}\text{H}_{28}\text{Cl}_5\text{NPRuS}$)

It has been synthesized using $[\text{RuCl}_3(\text{PPh}_3)_3]$ and 4-(3-chlorophenyl)-2-(4-chlorophenyl)-6-(thiophen-2-yl)pyridine as ligand (**L**⁵). Yield 19 %; m.p.: 259 °C; $\mu_{\text{eff}} = 1.91 \text{ B.M.}$; UV–Vis (DMSO): $\lambda_{\text{max}} = 551, 367, 271 \text{ nm}$.

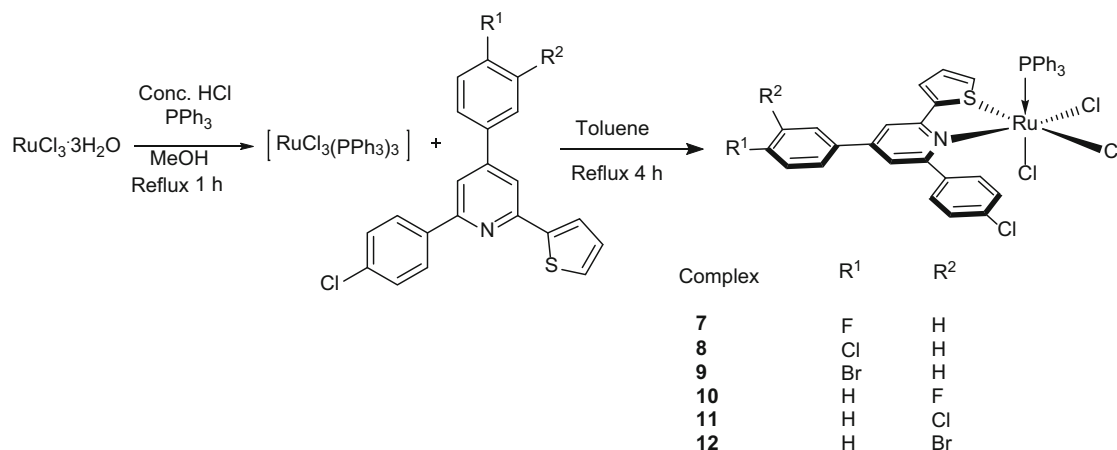
Trichloro[4-(3-bromophenyl)-2-(4-chlorophenyl)-6-(thiophen-2-yl)pyridine](triphenylphosphine)ruthenium(III) [$\text{RuCl}_3(\text{PPh}_3)\text{L}^6$] (**12**, $\text{C}_{39}\text{H}_{28}\text{BrCl}_4\text{NPRuS}$)

It has been synthesized using $[\text{RuCl}_3(\text{PPh}_3)_3]$ 4-(3-bromophenyl)-2-(4-chlorophenyl)-6-(thiophen-2-yl)pyridine (**L**⁶). Yield 18 %; m.p.: 278 °C; $\mu_{\text{eff}} = 1.92 \text{ B.M.}$; UV–Vis (DMSO): $\lambda_{\text{max}} = 558, 371, 270 \text{ nm}$.

In vitro antibacterial activity

The aim of this study was to evaluate in vitro bacterial potency of the ruthenium complexes against two Gram-positive (*Bacillus subtilis* and *Serratia marcescens*) and

Scheme 3



three Gram-negative (*Escherichia coli*, *Pseudomonas aeruginosa*, and *Staphylococcus aureus*). A broth dilution method was employed for screening antibacterial activity. A pre-culture of bacteria was used to prepare bacterial culture in Luria Broth. 50 cm³ of 2 % LB solution was prepared and sterilized after transferring 10 cm³ of its aliquots and definite concentration of test compounds into five corning tubes one for each bacterial species. Then 20 × 10⁻³ cm³ of bacterial culture from previously prepared control for each species was added into different corning tubes and inoculated for 24 h at 37 °C. This experiment is repeated until only a faint turbidity appears in the tube. The lowest concentration, which showed no visible growth after 24 h subculture was considered as MIC for each compound.

DNA binding mode investigation

UV-visible spectral titration of ruthenium complexes (in DMSO) with HS-DNA in phosphate buffer was carried out to inspect the binding mode for the complexes. In an experiment, fixed increment of DNA solution in phosphate buffer (100 × 10⁻³ cm³) was added to sample cell holding in definite concentration of complex solution (20 μM) and to the reference cell containing buffer and DMSO as a control to nullify the effect of DMSO in sample holding cell, and allowed to incubate for 10 min prior to the spectra being recorded [25–27]. The change in absorbance against wavelength at metal-to-ligand charge transfer (MLCT) band and intra-ligand transfer (ILT) band with increasing concentration of DNA was monitored to examine the binding strength in terms of intrinsic binding constant K_b . The intrinsic binding constant values was calculated using the following equation

$$\frac{[\text{DNA}]}{(\varepsilon_a - \varepsilon_f)} = \frac{[\text{DNA}]}{(\varepsilon_b - \varepsilon_f)} + \frac{1}{K_b(\varepsilon_b - \varepsilon_f)}$$

where ε_a , ε_f , and ε_b correspond to $A_{obsd}/[\text{complex}]$, the extinction coefficient for the free complex and the extinction coefficient for the complex in the fully bound form, respectively.

The binding of small molecules to DNA cannot be determined only by absorption titration method. Viscometric measurement is a supporting tool to confirm the binding mode. Viscosity measurements have been largely used to investigate the conformational changes of DNA induced by binding of complexes. In electrostatic and groove binding viscosity of DNA solution remain unaltered, while in classical intercalative binding viscosity will rise. Among these interactions, intercalation and groove binding are the most important DNA-binding modes as they invariably lead to cellular degradation. Herein, we carried out viscosity measurement at 37.0 ± 1 °C using a constant thermometric bath. To a solution of sonicated HS-DNA (approximately 200 bp) taken in Ubbelohde viscometer, a predetermined volume of the synthesized complex was supplemented. Subsequent to thorough agitation, resulting mixture was subjected to the measurement of relative viscosity. For each aliquot of the complex solution added, measurement was done thrice and average time was calculated. The relative viscosity ratio (η/η_0) has been plotted against the r -bound ($[\text{complex}]/[\text{DNA}]$) (where η and η_0 were the relative viscosity for DNA in the presence or absence of complexes, respectively). Viscosity measurements can sensitively detect the lengthening and unwinding of a DNA helix induced by the binding of intercalators [28], and thus provides evidence of intercalation for small DNA-binding molecules.

Brine shrimp lethality bioassay: a cytotoxicity profile

Cytotoxicity is the quality of being toxic to cells. Cytotoxicity assays are widely used by the pharmaceutical industry to screen for cytotoxicity in compound libraries. Researchers can look for cytotoxic compounds, if they are interested in developing a therapeutic that targets rapidly dividing cancer cells. Brine shrimp lethality assay is a method by which one can check the toxicity of the compounds on Brine Shrimp. The experiment was carried out following the protocol of Meyer et al. [29]. Set of 2, 4, 8, 16, and 20 $\mu\text{g cm}^{-3}$ were prepared from a stock solution of 1000 $\mu\text{g cm}^{-3}$ of the test compounds. Final volume in each test tube was adjusted to 2.5 cm^3 (1.0 cm^3 sea salt solution, 0.450 cm^3 double distilled water, 0.050 cm^3 DMSO + complex and remaining 1.0 cm^3 was added as 10 nauplii in a sea salt solution). After 24 h incubation, numbers of dead nauplii were counted and from the survival, % mortality was calculated.

Photochemical investigation of DNA nuclease activity

The impact of DNA cleavage in inorganic medicinal chemistry had motivated the researches to probe the coordination compounds that efficiently cleave the duplex DNA. Large interests have been drawn in transition metal mediated DNA cleavage studies [30, 31]. Whether the synthesized ruthenium complexes incorporating different substituted ligand vary in DNA cleavage ability was inspected using pUC19 DNA as a target employing electrophoresis. All the test samples were dissolved in DMSO. The samples were added to the isolated pUC19 DNA of *E. Coli* and incubated for 24 h before subjected to electrophoresis. System of 0.020 cm^3 (0.010 cm^3 DNA + 0.005 cm^3 test compound + 0.005 cm^3 quenching dye) for each test compound along with standard DNA marker containing TE buffer were loaded into the gel chamber wells and subjected to electrophoresis for 3–4 h maintaining a constant voltage of 100 V. The bands were visualized under UV illuminator and photographed to calculate the percentage cleavage of DNA.

Acknowledgments We are thankful to the Head of chemistry department and UGC RFSMS Scheme for providing financial support.

References

- Meggers E (2011) *Angew Chem Int Ed* 50:2442
- Meggers E (2009) *Chem Commun* 7:1001
- Rosenberg B, Vancamp L, Trosko J, Mansour V (1969) *Nature* 222:385
- Wheate N, Walker S, Craig G, Oun R (2010) *Dalton Trans* 39:8113
- Gallerani E, Bauer J, Hess D, Boehm S, Droege C, Jeckelmann S, Miani M, Herrmann R, Marsoni S, Sperka S, Sessa C (2011) *Acta Oncol* 50:1105
- Todd R, Lippard S (2009) *Metalomics* 1:280
- Galanski M, Jakupec M, Keppler B (2005) *Curr Med Chem* 12:2075
- Ott I, Gust R (2007) *Arch Pharm Chem Life Sci* 340:117
- Clarke M, Zhu F, Frasca D (1999) *Chem Rev* 99:2511
- Novakova O, Kasparkova J, Vrana O, Van Vliet P, Reedijk J, Brabec V (1995) *Biochemistry* 34:12369
- Velders A, Kooijman H, Spek A, Haasnoot J, De Vos D, Reedijk J (2000) *Inorg Chem* 39:2966
- Morris RE, Aird RE, del Socorro Murdoch P, Chen H, Cummings J, Hughes N, Parsons S, Parkin A, Boyd G, Jodrell D, Sadler P (2001) *J Med Chem* 44:3616
- Alessio E, Mestroni G, Bergamo A, Sava G (2004) *Curr Top Med Chem* 4:1525
- Hartinger C, Zorbas-Seifried S, Jakupec M, Zorbas H, Keppler B (2006) *J Inorg Biochem* 100:891
- Patel M, Patel C, Joshi H, Thakor K (2014) *Spectrochim Acta A* 127:261
- Pyle A, Rehmann J, Meshoyrer R, Kumar C, Turro N, Barton J (1989) *J Am Chem Soc* 111:3053
- Chao H, Mei W, Huang Q, Ji L (2002) *J Inorg Biochem* 92:165
- Sphillane C, Smith J, Buck D, Collins JG, Keene FR (2007) *Dalton Trans* 45:5290
- Friedman A, Chambron J, Sauvage J, Turro N, Barton J (1990) *J Am Chem Soc* 112:4960
- Xian-Lan H, Hong L, Cui-Hong P (2011) *J Mol Struct* 990:197
- Li-Feng T, Hui C, Kang-Cheng Z, Jun-Jie F, Fang W, Yang-Fan Z, Liang-Nian J (2007) *Polyhedron* 26:5458
- Krohnke F (1976) *Synthesis* 1976:1
- Garza-Ortiz A, Maheswari PU, Sieglar M, Spek A, Reedijk J (2013) *New J Chem* 37:3450
- Ruminski R, Kahrilas G, Schauer B (2015) *Inorg Chim Acta* 430:184
- Barton J, Dannenberg J, Raphael A (1984) *J Am Chem Soc* 106:2172
- Smith S, Neyhart G, Karlsbeck W, Thorp H (1994) *New J Chem* 18:397
- Carter M, Rodrigues M, Bard A (1989) *J Am Chem Soc* 111:8901
- Leng F, Priebe W, Chaires J (1998) *Biochemistry* 37:1743
- Meyer B, Ferrigni N, Putnam J, Jacobsen L, Nichols D, McLaughlin J (1982) *Planta Med* 45:31
- Hertzberg R, Dervan P (1982) *J Am Chem Soc* 104:313
- Sigman D, Graham D, Marshall L, Reich K (1980) *J Am Chem Soc* 102:5419